Elevated pyramidal cell firing orchestrates arteriolar vasoconstriction through COX-2-derived prostaglandin E2 signaling

B Le Gac[1], M Tournissac[2], Belzic E[1], S Picaud[1], I Dusart[1], H Soula[3], D Li[1], S Charpak[2], B Cauli[1*]

1. Sorbonne Université, CNRS, INSERM, Neurosciences Paris Seine - Institut de Biologie Paris Seine (NPS-IBPS), 9 quai Saint Bernard, 75005 Paris, France.

2. Sorbonne Université, INSERM, CNRS, Institut de la Vision, 17 rue Moreau, 75012 Paris, France.

3. Sorbonne Université, INSERM, Nutrition and Obesities: Systemic Approaches, NutriOmics, research unit, 91 boulevard de l'hôpital, 75013 Paris, France.

*Correspondence: bruno.cauli@upmc.fr

Classification: Biological Sciences, Pharmacology

Keywords: Neurovascular coupling, pyramidal cells, prostaglandin E2 signaling, optogenetics

ABSTRACT

Neurovascular coupling (NVC), linking neuronal activity to cerebral blood flow (CBF), is essential for brain function and underpins functional brain imaging. Whereas mechanisms involved in vasodilation are well-documented, those controlling vasoconstriction remain overlooked. This study unravels the mechanisms by which pyramidal cells elicit arteriole vasoconstriction. Using patch-clamp recording, vascular and Ca^{2+} imaging in Emx1-Cre;Ai32 mouse cortical slices, we show that strong optogenetic activation of layer II/III pyramidal cells induces arteriole vasoconstriction, correlating with firing frequency and somatic Ca^{2+} increase. *Ex vivo* and *in vivo* pharmacological investigations indicate that this neurogenic vasoconstriction extends beyond glutamatergic transmission and predominantly recruits prostaglandin E2 (PGE2) through the cyclooxygenase-2 (COX-2) pathway, and activation of EP1 and EP3 receptors. Single-cell RT-PCR further identifies layer II/III pyramidal cells as a key source of COX-2-derived PGE2. Additionally, we present evidence that specific neuropeptide Y (NPY) interneurons acting on Y1 receptor, and astrocytes, through 20-hydroxyeicosatetraenoic acid (20-HETE) and COX-1-derived PGE2, contribute to this process. By revealing the mechanisms by which the activity of pyramidal cells leads to vasoconstriction, our findings shed light on the complex regulation of CBF.

Significance statement

Cerebral blood flow is tightly controlled by neuronal activity, a process termed neurovascular coupling which serves as the physiological basis for functional brain imaging widely used to map neuronal activity in health and diseases. While the prevailing view links increased neuronal activity with enhanced blood perfusion, our data suggest that elevated neuronal activity can also reduce cerebral blood flow. By optically controlling the activity of pyramidal cells, we demonstrate that these excitatory neurons induce vasoconstriction when their action potential firing is increased by releasing glutamate and lipid messengers. These findings update the interpretation of functional brain imaging signals and help to better understand the etiopathogenesis of epilepsy and Alzheimer's disease, in which hyperactivity, hypoperfusion and cognitive deficits overlap.

Introduction

The brain critically depends on the uninterrupted blood supply provided by a dense vasculature[1]. Cerebral blood flow (CBF) is locally and temporally controlled by neuronal activity, this essential process is called neurovascular coupling (NVC), and is impaired in early stages of numerous neurological disorders[2]. NVC also serves as the physiological basis for functional brain imaging widely used to map neuronal activity. Increased neuronal activity increases CBF within seconds[2]. In the cerebral cortex, the hyperemic response linked to neural activity is supported by dynamically controlled vasodilation that is spatially and temporally restricted by delayed vasoconstriction in the surrounding area[3]. Conversely, vasoconstriction and decreased CBF usually correlate with reduced neuronal activity[3,4].

However, mounting evidence indicates that under physiological conditions the positive correlation between neuronal activity and CBF is not always met. For instance, i) robust sensory-evoked vasodilation can occur in the absence of substantial neuronal response[5], ii) conversely, pronounced neuronal activity is not systematically associated with increased hemodynamics[6], iii) CBF is decreased in several cortical areas despite local increase in neuronal activity[7] and iv) optogenetic simulation of inhibitory GABAergic interneurons results in vasodilation[8]. Furthermore, in pathological conditions with intense neuronal activity such as epileptic seizures, a sustained hypoperfusion/vasoconstriction is observed[9,10].

NVC is achieved by the synthesis and release of vasoactive messengers within the neurovascular unit[2], which act on the contractility of mural cells (smooth muscle cells and pericytes) to control vessel caliber and CBF along the vascular tree[11]. Pial and penetrating arterioles, which have a higher density of contractile mural cells and control their diameter faster than capillaries[11–14], play a key role in regulating CBF. Messengers of vasodilation released by excitatory neurons, GABAergic interneurons, astrocytes, or endothelial cells, include nitric oxide, K^+, arachidonic acid derivatives such as prostaglandin E2 (PGE2)[2], or more recently glutamate[15]. Despite its physio pathological importance, vasoconstriction is less understood with fewer cell types and vasoactive messengers that have been identified. It is now generally accepted that GABAergic interneurons are key players in vasoconstriction by releasing neuropeptide Y (NPY)[8,16]. However, under certain conditions astrocytes can also induce vasoconstriction via 20-hydroxyeicosatetraenoic acid (20-HETE)[17] or high K^+

concentration[18]. The involvement of pyramidal cells in the process remains to be investigated.

PGE2 has emerged as a bimodal messenger of NVC, similar to K^{+}[18] and glutamate[15], that can induce either vasodilation[19–22] or vasoconstriction[23,24] depending on its concentration and/or site of action along the vascular tree. Under physiological conditions, PGE2 is produced during NVC by either astrocytes[21] or pyramidal cells[22] via the rate-limiting synthesizing enzymes cyclooxygenase-1 (COX-1) or -2 (COX-2), respectively. Since COX-2-expressing pyramidal cells can release glutamate and PGE2, both of which induce vasoconstriction at high concentrations[15,23,24], pyramidal cells may be responsible for vasoconstriction when their spiking activity is high.

To test this hypothesis, we used *ex vivo* and *in vivo* approaches in combination with optogenetics to precisely control pyramidal cell firing in the mouse barrel cortex while monitoring the resulting arteriolar response. We found that pyramidal cells induce vasoconstriction at high stimulation frequency and express all the transcripts required for a cell autonomous synthesis of the vasoconstrictor messengers, PGE2 and prostaglandin F2α (PGF2α). Pharmacological investigations revealed that this neurogenic vasoconstriction depends on COX-2-derived PGE2 via the direct activation of vascular EP1 and EP3 receptors. It also involves the recruitment of intermediary NPY interneurons acting on the Y1 receptor, and, to a lesser extent astrocytes, via 20-HETE and COX-1-derived PGE2. Thus, our study reveals the mechanisms by which high frequency pyramidal cell firing leads to vasoconstriction.

Results

Pyramidal cells induce vasoconstriction at high firing frequency.

To determine if pyramidal cells action potential (AP) firing can induce vasoconstriction in a frequency-dependent manner, we used optogenetics to induce AP firing while monitoring the resulting vascular response in cortical slices. We used Emx1-cre;Ai32 transgenic mice expressing the H134R variant of channelrhodopsin-2 (ChR2) in the cortical glutamatergic neurons[25], conferring robust pyramidal cell photoexcitability[26]. Wide-field photostimulation of cortical slices was achieved in layers I to III (Supplementary Fig. 1a) using 10-second trains

88 of 5 ms light pulses (see Methods) delivered at five different frequencies (1, 2, 5, 10 and 20
89 Hz, Fig. 1a).

90 First, we ensured the efficiency of the photostimulation paradigm by recording layer II-III
91 pyramidal cells in whole-cell current clamp mode (Fig. 1a). We observed that optogenetic
92 stimulation resulted in the firing of an initial AP that was followed by a train of spikes whose
93 amplitude and frequency transiently decreased before reaching a steady state (Fig. 1a, upper
94 traces). Consistent with the kinetic properties of the H134R ChR2 variant[27] and the intrinsic
95 firing properties of pyramidal cells[28], the steady-state firing frequency matched the
96 photostimulation frequency up to 5 Hz but was lower at higher frequencies (Fig. 1a, steady-
97 state spike success rate: 100 ± 0 % at 1, 2 and 5 Hz, 70 ± 11 % at 10 Hz and 55 ± 12 % at 20
98 Hz). These observations demonstrate efficient pyramidal cell activation over a wide range of
99 photostimulation frequencies.

100 To test the prediction that neuronal activity induces vasoconstriction, we visualized the
101 optogenetically-induced response of penetrating arterioles. Layer I arterioles were imaged
102 for 30 minutes in cortical slices (Supplementary Fig.2; Supp. table 1) without preconstriction
103 to facilitate observation of vasoconstriction[16]. Examination of the evoked vascular response
104 over 30-minutes (Supplementary Fig.2) showed that increasing the frequency of
105 photostimulation shifted the overall vascular response from a barely discernible delayed
106 response between 1 Hz and 5 Hz to a sustained vasoconstriction at 10 Hz and above. This
107 tendency was particularly pronounced at 20 Hz, with most vessels (n= 8 of 10 arterioles)
108 showing a strong and rapid vasoconstriction. On average, this response peaked at 6.8 ± 2.4
109 min, much earlier than at lower frequencies, which typically required more than 10 min to
110 reach a maximum (Supplementary Fig.2c, 1 Hz: 15.6 ± 4.0 min; 2 Hz: 13.2 ± 2.3 min; 5 Hz:
111 16.0 ± 3.6 min; 10 Hz: 15.7 ± 2.4 min). Because the vascular response shifted to reliable
112 vasoconstriction in less than 10 minutes when the frequency of photostimulation was
113 increased to 20 Hz, we defined the first 10 minutes of recording as the vasoconstriction time
114 frame for subsequent comparisons and analyses. While photostimulation at 1 to 5 Hz failed
115 to elicit fast reliable vascular responses (Fig. 1c-d), 10 Hz photostimulation predominantly
116 induced vasoconstriction (n= 4 of 5 arterioles, Fig. 1 c-d, area under the curve (AUC)= -1.7 ±
117 1.1 x 10^3 %.s, n= 5). This response was even more pronounced at 20 Hz, as all arterioles
118 showed vasoconstriction of high magnitude (Fig. 1 b-d; AUC= -3.7 ± 0.7 x 10^3 %.s, $F_{(4, 30)}$=

119 6.135, p= 9.89 x 10^{-4}, one-way ANOVA, n= 10 arterioles). This difference was particularly
120 striking when comparing the magnitude at 20 Hz (Fig. 1d) with those at 1 Hz ($t_{(12)}$= -3.48, p=
121 0.0407, t-test), 2 Hz ($t_{(18)}$= -4.09, p= 0.0250, t-test) and 5 Hz ($t_{(14)}$= -3.7, p= 0.0346, t-test).
122 Intense optogenetic stimulation of pyramidal cells has been shown to elicit cortical
123 spreading depression[29], which induces vasoconstriction[15] and fast cell swelling[30]. We ruled
124 out this possibility by showing that the rate of change in light transmittance associated with
125 cell swelling remained below that of cortical spreading depression[30] (Supplementary Table
126 1). On the other hand, ChR2-independent vascular changes induced by high light intensity
127 have been reported[31]. We verified that 20 Hz photostimulation did not induce a vascular
128 response in wild-type mice that do not express ChR2 (Supplementary Fig.1). Taken together,
129 our observations indicate that photostimulation of pyramidal cells produces a frequency-
130 dependent vasoconstriction that occurs and amplifies at high firing rates.

131 **Optogenetic stimulation induces a frequency-dependent, gradual increase in somatic**
132 **calcium that precedes the vascular response.**

133 These observations raise the questions of how pyramidal neurons can induce
134 vasoconstriction at higher AP-firing rates. It is generally accepted that the synthesis and/or
135 release of vasodilatory substances requires an increase in intracellular Ca^{2+} in the releasing
136 cells[32,33], but little is known about the release of vasoconstricting substances. We therefore
137 determined whether an increase in somatic Ca^{2+} concentration in cortical neurons was also
138 dependent on photostimulation frequency. We combined optogenetic stimulation with
139 whole-cell current clamp recording and intracellular Ca^{2+} imaging using Rhod-2 delivered by
140 patch pipette (Fig. 2a). Excitation of this red Ca^{2+} indicator at 585 nm did not induce any
141 voltage response in the recorded pyramidal cells (Fig. 2a and supplementary Fig. 3), as
142 expected from the action spectrum of ChR2[27]. In contrast, photostimulation at 470 nm
143 elicited a train of spikes accompanied by a somatic Ca^{2+} increase that lasted tens of seconds
144 following photostimulation without triggering any significant recurrent spiking activity
145 (Supplementary Fig. 3). The Ca^{2+} response evoked by 20 Hz photostimulation was more than
146 twice of that evoked by 2 Hz photostimulation (Fig. 2b; 2 Hz: $\Delta F/F_0$= 34.5 ± 3.7 %, n= 9 cells,
147 vs. 20 Hz: $\Delta F/F_0$= 79.5 ± 17.7 %, n= 9 cells; $t_{(16)}$= 2.485, p= 0.024397), while the average
148 number of evoked spikes was about five times higher (Fig. 1a and supplementary Fig. 3).
149 These results demonstrate a frequency-dependent increase in intracellular Ca^{2+} induced by

150 photostimulation, that is temporally compatible with the synthesis and/or release of
151 vasoactive mediators and subsequent vasoconstriction. We therefore aimed to understand
152 the molecular mechanisms linking neuronal activity to vasoconstriction.

153 **Vasoconstriction induced by pyramidal cells requires spiking activity and is only partially**
154 **dependent on glutamatergic transmission.**

155 In pyramidal cells, APs induce both somatic Ca^{2+} elevation[34] and glutamate release. To
156 determine whether spiking activity is required for vasoconstriction induced by 20 Hz
157 photostimulation, we blocked APs with the voltage-activated sodium channel blocker
158 tetrodotoxin (TTX, 1 µM, n= 6 arterioles). This treatment completely abolished the
159 vasoconstriction evoked by 20 Hz photostimulation (Fig. 3; AUC= 0.4 ± 0.4 x 10^3 %.s, $t_{(14)}$=
160 5.57, p= 8.6656 x 10^{-6}). These data indicate that APs are mandatory for neurogenic response
161 and may involve glutamate release.

162 Indeed, high levels of glutamate released from pyramidal cells may activate vasoconstrictive
163 cells, including NPY-expressing interneurons or astrocytes, through activation of ionotropic
164 or group I metabotropic glutamate receptors[8,17,18]. It may also directly activate NMDA
165 receptors on arteriolar smooth muscle cells, resulting in a large intracellular Ca^{2+} increase
166 and subsequent vasoconstriction[15]. To test the hypothesis that glutamate from pyramidal
167 cells, either directly or indirectly, results in vasoconstriction, we blocked glutamatergic
168 transmission by antagonizing AMPA/kainate, NMDA and group I metabotropic receptors
169 expressed by cortical neurons[35,36] and juvenile astrocytes[37]. Glutamate receptor antagonists
170 reduced the magnitude of vasoconstriction (-1.6 ± 0.4 x 10^3 %.s, $t_{(18)}$= 3.28, p= 0.0160) by
171 approximately half (Fig. 3). Taken together, our data suggest that photostimulation of
172 pyramidal cells elicits a frequency-dependent vasoconstriction that requires their spiking
173 activity and partially involves glutamatergic transmission. We therefore sought to elucidate
174 the glutamate-independent vasoactive pathway underlying this neurogenic vascular
175 response.

176 **Pyramidal cells express the mRNAs for a cell autonomous PGE2 and PGF2α synthesis**

177 Several arachidonic acid metabolites produced after intracellular Ca^{2+} elevation, including
178 PGF2α, but also PGE2, exert dose-dependent vasoconstrictive effects[23,24,38]. These
179 prostaglandins could therefore be progressively released as the frequency of

180 photostimulation and somatic Ca^{2+} increase, and thereby promote vasoconstriction. Layer II-
181 III pyramidal cells have been shown to produce PGE2[22]. To determine whether the
182 synthesizing enzymes of PGE2 and PGF2α are present in pyramidal cells, we performed
183 single-cell RT-PCR after patch-clamp recording[39]. Sixteen layer II-III pyramidal cells were
184 visually identified based on the triangular shape of their soma and a prominent apical
185 dendrite. Their glutamatergic phenotype was confirmed both by their stereotypical regular
186 spiking firing pattern (Fig. 4a) and also by the expression of the vesicular glutamate
187 transporter, vGlut1, and neither of the two GABA synthesizing enzymes (Fig. 4b)[28]. The rate-
188 limiting enzymes of prostaglandin synthesis, cyclooxygenase-1 (COX-1) and -2 (COX-2), were
189 detected in 25% (n= 4 of 16 cells) and 31% (n= 5 of 16 cells) of pyramidal cells, respectively,
190 (Fig. 4b-d) but were never co-expressed (Fig. 4d). The cytosolic enzyme responsible for
191 synthesizing PGE2 (cPGES) was observed in most pyramidal cells (Fig. 4b-c; 88%, n= 14 of 16
192 cells). In addition, the microsomal PGES, mPGES1 and mPGES2 were detected in 6% (Fig. 4c,
193 n= 1 of 16 cells) and 38% (Fig. 4b,c; n= 6 of 16 cells) of pyramidal cells, respectively, and were
194 always co-expressed with cPGES. The PGF2α terminal-synthesizing enzyme AKR1B3 was
195 observed in the majority of neurons (Fig. 4b-c; n= 11 of 16 cells, 69%). Occasionally, it was
196 co-detected with the prostamide/prostaglandin F synthase (PM-PGFS, Fig. 4c, n= 5 of 16
197 cells, 31%) and the PGE2 converting enzyme carbonyl reductase 1 (CBR1, Fig. 4c; n= 3 of 16
198 cells, 19%). CBR1 was consistently detected alongside at least one PGES. Pyramidal cells
199 positive for COX-1 also expressed PGES (Fig. 4d), with most of them also co-expressing PGFS
200 (n=3 out of 4). All neurons positive for COX-2 co-expressed both PGES and PGFS (Fig. 4d).
201 These molecular observations suggest that subpopulations of layer II-III pyramidal cells
202 express all the necessary transcripts for the synthesis of PGE2 and PGF2α .

203 **Prostaglandins underpin vasoconstriction *ex vivo* and *in vivo*.**

204 To investigate whether prostaglandins could mediate neurogenic vasoconstriction, we
205 inhibited their synthesis. The non-selective COX inhibitor indomethacin (5 µM,
206 supplementary Table 3, Fig. 5a) completely abolished the vascular response (n= 10
207 arterioles, AUC= 0.0 ± 0.2 x 10^3 %.s, $t_{(18)}$= 5.86, p= 3.4385 x 10^{-5}). *In vivo* monitoring of pial
208 artery diameter changes by 2-photon imaging (Fig. 5c and d) during 10 Hz photostimulation
209 of anesthetized Emx1-cre;Ai32 mice revealed that pyramidal cells induce vasodilation
210 followed by sustained vasoconstriction (Fig. 5d and e). This confirms and expands upon

211 previous *in vivo* observations[8]. The constriction phase was inhibited by indomethacin (i.v.),
212 indicating the involvement of prostaglandins in the vasoconstriction (AUC_{Ctrl}= -291.5 ± 92.4
213 %.s vs. $AUC_{Indo.}$= 332.4 ± 184.4 %.s, $U_{(5,4)}$= 0, p= 0.0159, Fig. 5d-f), which confirms our *ex vivo*
214 observations. To determine whether they originated from COX-1 or COX-2 activity, we
215 utilized selective inhibitors. The vasoconstriction magnitude was reduced by the COX-1
216 inhibitor SC-560 (100 nM, n= 10 arterioles, supplementary Table 3) (-1.4 ± 0.7 x 10^3 %.s, $t_{(18)}$=
217 3.54, p= 9.3396 x 10^{-3}, Fig. 5b-c). The COX-2 inhibitor NS-398 (10 µM, n= 7 arterioles,
218 supplementary Table 3) completely abolished pyramidal cell-induced vasoconstriction in a
219 more potent manner (Fig. 5b; AUC= 0.1 ± 0.3 x 10^3 %.s, $t_{(15)}$= 5.45, p= 1.0853 x 10^{-5}). These
220 observations suggest that prostaglandins, derived mainly from COX-2 activity, and to a lesser
221 extent from COX-1 activity, mediate pyramidal cell-induced vasoconstriction.

222 **PGE2 mediates vasoconstriction by acting primarily on EP1 receptor.**

223 To determine the nature of the prostaglandins and their receptors, we selectively
224 antagonized the vasoconstrictor receptors of PGE2, EP1 or EP3, or the FP receptor of PGF2α.
225 The magnitude of vasoconstriction was reduced by the selective EP1 receptor antagonist
226 ONO-8130 (10 nM, n= 9 arterioles, Fig. 6, 0.3 ± 0.3 x 10^3 %.s, $t_{(17)}$= 6.01, p= 2.8451 x 10^{-6},
227 supplementary Table 3), and to a lesser extent, by the EP3 receptor antagonist L-798,106 (1
228 µM, n= 9 arterioles, Fig. 6, -0.9 ± 0.4 x 10^3 %.s, $t_{(17)}$= 4.30, p= 8.0261 x 10^{-4}, supplementary
229 Table 3). Impairing FP receptor signaling with AL-8810 (10 µM, n= 9 arterioles, Fig. 6,
230 Supplementary table 3) tended to reduce the evoked vasoconstriction, however, it did not
231 reach statistical significance (AUC= -1.9 ± 0.4 x 10^3 %.s, $t_{(17)}$= 2.82, p= 0.0533). Additionally,
232 the pre-constricted state induced by this weak partial FP agonist[40] (supplementary Fig. 6f)
233 resulted in a diameter reduction of approximately 4% (diameter before application 21.8 ±
234 2.5 µm vs. during 20.9 ± 2.6 µm, n= 9 arterioles, $t_{(8)}$= 2.374, p= 0.0457, paired t-test), which
235 underestimated the optogenetic vascular response. Taken together, these results indicate
236 that pyramidal cell photoactivation induces vasoconstriction through the release of PGE2
237 originating from COX-2. This effect primarily acts on the EP1 receptor and, to a lesser extent,
238 on the EP3 receptor.

239 To test a direct effect of PGE2 through vascular EP1/EP3 activation, we determined whether
240 exogenous agonists of PGE2 receptors could mimic the vasoconstriction induced by
241 pyramidal cell photostimulation. Similar to increasing photostimulation frequencies,

242 exogenous application of PGE2 induced vasoconstriction in a dose dependent manner
243 (Supplementary Fig. 7a). Likewise, 10 µM sulprostone, an EP1/EP3 agonist with an EC_{50}
244 comparable to that of PGE2[41], mimicked the vasoconstriction induced by 1-10 µM PGE2
245 (Supplementary Fig. 7b). Application of 10 µM PGE2 in the presence of TTX did not impair
246 the evoked vasoconstriction (Supplementary Fig. 7c). These observations suggest that PGE2
247 and its EP1 and EP3 receptors mediate the neurogenic vasoconstriction and that once PGE2
248 is released, its vascular effect is independent of spiking activity.

249 **Astrocytes through 20-HETE and NPY interneurons are indirect intermediates of pyramidal**
250 **cell-induced vasoconstriction.**

251 In addition to smooth muscle cells, PGE2 released by pyramidal cells can also activate
252 astrocytes and neurons[42,43], which also express its receptors[35,36]. To assess whether
253 astrocytes could mediate the PGE2-dependent vasoconstriction, we first targeted the large
254 conductance Ca^{2+}-activated (BK) channels and the 20-HETE pathways, both of which mediate
255 astrocyte-derived vasoconstriction dependent on glutamatergic transmission[17,18]. Blockade
256 of BK channels with paxilline (1 µM, n= 10 arterioles, Supplementary table 3) did not impair
257 the vascular response (Fig. 7; AUC = -3.7 ± 0.3 x 10^3 %.s, $t_{(18)}$ = 0.03, p = 1). Selective
258 inhibition of the 20-HETE synthesizing enzyme, CYP450 ω-hydroxylase, with HET-0016 (100
259 nM, n= 10 arterioles, Supplementary table 3) reduced the magnitude of the evoked
260 vasoconstriction (Fig. 7; AUC = -1.6 ± 0.7 x 10^3 %.s, $t_{(18)}$ = 3.32, p = 0.0160). These data
261 suggest that astrocytes partially mediate the vasoconstriction induced by pyramidal cells via
262 20-HETE but not via K^+ release. We next determined whether NPY, a potent
263 vasoconstrictor[16], was involved in neurogenic vasoconstriction. Antagonism of the NPY Y1
264 receptors by BIBP3226 (1 µM, n= 10 arterioles, Supplementary table 3) completely abolished
265 neurogenic vasoconstriction (Fig. 6; AUC = -0.3 ± 0.2 x 10^3 %.s, $t_{(18)}$ = 5.28, p = 1.9512 x 10^{-5}).
266 These results suggest that neurogenic vasoconstriction induced by pyramidal cells
267 photostimulation involves the activation of NPY-expressing interneurons and Y1
268 receptors[8,16,28] and astrocytes via 20-HETE in glutamatergic-dependent and -independent
269 manners.

Discussion

This study establishes that pyramidal cells activity leads to arteriole vasoconstriction, and the magnitude of the vasoconstriction depends on AP firing frequency and correlates with a graded increase in pyramidal cell somatic Ca^{2+}. This vascular response requires AP firing and partially involves glutamatergic transmission through direct and indirect mechanisms on arteriolar smooth muscle cells. *Ex vivo* and *in vivo* observations revealed that PGE2, predominantly produced by layer II-III COX-2 pyramidal cells, and its EP1 and EP3 receptors play a crucial role in neurogenic vasoconstriction. Pharmacological evidence indicates that some interneurons, via NPY release and activation of Y1 receptors, and to a lesser extent, astrocytes through 20-HETE and possibly COX-1 derived PGE2 play an intermediary role in this process (Figure 8).

We found that increasing the frequency of photostimulation in an ex vivo preparation caused nearby arteriole to go from a barely discernible response to robust vasoconstriction. In contrast, *in vivo* observations have shown that the optogenetic stimulation of pyramidal cells induces a hyperemic/vasodilatory response[22,44,45], that can be followed by vasoconstriction[8]. This biphasic response was confirmed *in vivo.* However, a more pronounced vasoconstriction phase was observed when using high frequency 10-second-long periods of photostimulation (Fig. 5). The difficulty in observing vasodilation in cortical slices may be due to relaxed arterioles which favor vasoconstriction[46]. However, the evidence that neurogenic vasoconstriction is frequency-dependent (Fig. 1) and that pharmacologically-induced vasoconstriction persists in preconstricted[18] or pressurized arterioles[24], suggests that the neurogenic vasoconstriction primarily depends on a high pyramidal cell firing rate rather than on vascular tone. The mandatory role of action potentials indicates that Ca^{2+} entry via ChR2 alone is insufficient to drive a vascular response. This likely reflects the essential role of voltage-gated Ca^{2+} channels in somatic Ca^{2+} elevation[47] and the subsequent release of neuronal vasoactive agents[8,22].

Most previous observations did not report a decreased in CBF induced by optogenetic stimulation of pyramidal cells *in vivo*[22,45]. This may be attributed to differences in the photostimulation paradigm and/or the specific subtype of pyramidal cells that were stimulated. In our study, we used 10 seconds of photostimulation both *in vivo* and *ex vivo*. Earlier studies have employed shorter photostimulation times, lasting no more than 1

301 second[8,22,45], which may have resulted in an insufficient number of elicited APs to induce
302 robust vasoconstriction. Furthermore, we observed that neurogenic vasoconstriction is
303 highly dependent on COX-2, which is primarily expressed in layer II-III pyramidal cells[22,35,36].
304 In our study, photostimulation of almost all pyramidal cells in Emx1-Cre;Ai32 mice[25,26] likely
305 resulted in the release of more COX-2 metabolites. Thy1-ChR2 mice used in previous
306 studies[8,45], on the other hand, express primarily ChR2 in layer V pyramidal cells[44,] which
307 rarely express COX-2.

308 Our *ex vivo* and *in vivo* observations revealed that PGE2, primarily derived from COX-2, plays
309 a critical role in neurogenic vasoconstriction by activating EP1 and EP3 receptors expressed
310 by vascular smooth muscle cells[15]. Previous studies have shown that COX-2 pyramidal cells,
311 when activated *in vivo* by sensory stimulation or *ex vivo*, induce a NMDA-dependent increase
312 in CBF and vasodilation through PGE2 and EP2/EP4 receptors[19,22,48]. Differences in the levels
313 and/or sites of action of released PGE2 may explain the absence of secondary
314 vasoconstriction. In Emx1-Cre;Ai32 mice[25,26], optogenetic stimulation may have activated a
315 greater number of COX-2 pyramidal cells and resulted in a higher local release of PGE2
316 compared to sensory stimulation. A high level of PGE2 may have facilitated the activation of
317 the EP1 receptor, which has a lower affinity than the EP2/EP4 receptors[41]. Additionally, it
318 may have promoted the rapid desensitization of the dilatory EP4 receptor[49] thereby favoring
319 vasoconstriction. Furthermore, PGE2 can induce either EP1-dependent arteriolar dilation or
320 constriction depending on whether it is locally applied to capillaries or arterioles.
321 Constriction prevails when both segments are exposed[23]. Our photostimulation focused on
322 superficial penetrating arterioles, which lack a capillary network in their close vicinity[50]. This
323 may have facilitated the direct EP1-mediated arteriolar constriction[23,24]. Overall, these
324 observations suggest that COX-2 pyramidal cells can sequentially promote both vasodilation
325 and vasoconstriction through the release of PGE2, depending on the context.

326 Consistent with previous reports in rodents[22,35,36,51], the transcripts of the rate-limiting
327 enzymes COX-1 and COX-2, were detected in subpopulations of mouse layer II-III pyramidal
328 cells, respectively. COX-1/2 expression was found to be systematically associated with at
329 least one PGE2 synthesizing enzyme. The major isoforms were cPGES and mPGES2, with the
330 latter being less prevalent[22,35,36]. The low detection rate of mPGES1, an isoform co-induced
331 with COX-2 by various stimuli[52,53], reflects its low constitutive basal expression level. The

332 presence of PM-PGFS, CBR1 and AKR1B3 in layer II-III pyramidal cells is consistent with
333 single-cell RNAseq data[35,36]. The expression of a PGFS was systematically observed in COX-2
334 positive pyramidal cells and in a majority of COX-1 positive neurons, similar to PGES. These
335 observations collectively indicate that subpopulations of layer II-III pyramidal cells express
336 the mRNAs required for PGE2 and PGF2α synthesis derived from COX-1 or COX-2 activity.
337 Our pharmacological observations did not reveal a contribution of PGF2α in neurogenic
338 vasoconstriction, despite the potential ability of pyramidal cells to produce it. This is likely
339 because PGF2α is only detectable in pyramidal neurons under conditions where COX-2 is
340 over-expressed[54].

341 Pyramidal cells may have an indirect effect on vascular activity through the activation of
342 intermediate cell types, in addition to the direct vascular effects of PGE2 and glutamate[15.]
343 Consistent with previous observations, we found that glutamate transmission from
344 pyramidal cells is involved to some extent[8]. Additionally, we found that the NPY Y1 receptor
345 plays a key role in neurogenic vasoconstriction. It is likely that glutamatergic transmission
346 contributed to NPY release, considering that NPY GABAergic interneurons express a wide
347 range of ionotropic and metabotropic glutamate receptors[35,36]. Consistently, the Y1 receptor
348 has been shown to be involved in vasoconstriction induced by sensory and optogenetic
349 stimulation of GABAergic interneurons[8]. This vascular response originates in deep layers and
350 propagates upstream to the pial surface. The density of neuronal-arteriolar smooth muscle
351 cell junctions[15] and of NPY interneurons[35] is higher in deep layers, supporting an initial
352 activation in those layers. However, layer I contains numerous NPY interneurons[28,35] and
353 exhibits strong Y1 receptor immunoreactivity in smooth muscle cells[55]. This suggests that
354 neurogenic vasoconstriction may also be relayed by superficial NPY interneurons.

355 Activation of group I metabotropic receptors in perivascular astrocytes has been shown to
356 promote vasoconstriction via BK channel-dependent K^+ release[18] or 20-HETE[17]. However, the
357 neurogenic vasoconstriction was not affected by the blockade of BK channels, which rules
358 out this astrocytic pathway. In contrast, the inhibition of ω-hydroxylase partially reduced
359 neurogenic vasoconstriction, suggesting the involvement of 20-HETE. Additionally,
360 astrocytes may also have contributed to vasoconstriction through the release of PGE2
361 derived from COX-1[56], as indicated by its mild impairment under SC-560. Pyramidal cells may
362 have indirectly contributed to neurogenic vasoconstriction via the release of PGE2, in

363 addition to glutamate. Indeed, GABAergic interneurons and astrocytes express PGE2
364 receptors[35,36], and PGE2 has been shown to induce neuronal firing and increase Ca^{2+} levels in
365 astrocytes[42,43]. Therefore, glutamate and PGE2 released from pyramidal cells may act
366 synergistically to indirectly promote vasoconstriction.

367 Although the vasoconstriction observed in epilepsy[9], shares similar mechanisms with the
368 neurogenic vasoconstriction described here, it differs in several aspects. Epileptic seizures
369 induce long-lasting hypoperfusion leading to severe hypoxia and memory and cognitive
370 impairment[9]. The high level of glutamate associated with epilepsy is likely to contribute to
371 the direct contraction of smooth muscle cell[15]. Like neurogenic vasoconstriction, seizure-
372 induced hypoperfusion is dependent on COX-2[9,10] and, to some extent on PGE2[9], likely
373 through EP1 and/or EP3 receptors. However, epileptic seizures induce the overexpression of
374 both COX-2 and mPGES1[51,53]. Additionally, PGF2α synthesis by COX-2 pyramidal cells is also
375 produced during seizures[54], suggesting that PGF2α and the FP receptors may also be
376 involved in this hypoperfusion.

377

378 Here, using multidisciplinary approaches, we describe a new mechanism of vasoconstriction
379 that depends on a high firing rate of pyramidal cells. This neurogenic vasoconstriction
380 primarily involves the release of COX-2-derived PGE2 and activation of EP1 and EP3
381 receptors. It is mediated by direct effects on vascular smooth muscle cells but also by
382 indirect mechanisms involving NPY release from GABAergic interneurons and astrocytes by
383 20-HETE synthesis. In contrast to previously described mechanisms of neurogenic
384 vasoconstriction, that have been mostly associated with GABAergic interneurons and
385 neuronal inhibition[3,8,16,57,58], our data suggest the involvement of glutamatergic excitatory
386 neurons and increased neuronal activity. This finding will help to update the interpretation
387 of the functional brain imaging signals used to map network activity in health and disease[2,59].
388 This excitatory form of neurogenic vasoconstriction may also help to understand the
389 etiopathogenesis of epilepsy[9,10] and Alzheimer's disease[60] in which increased cortical
390 network activity and hypoperfusion often overlap.

391 **Methods**

392 **Animals**

393 Homozygous Emx1-Cre mice [Jackson Laboratory, stock #005628, B6.129S2-Emx1$^{tm1(cre)Krj}$/J
394 [25]] were crossed with homozygous Ai32 mice [Jackson Laboratory, stock #012569, B6;129S-
395 Gt(ROSA)26Sor$^{tm32(CAG-COP4*H134R/EYFP)Hze}$/J [26]] to obtain heterozygous Emx1$^{cre/WT}$;Ai32$^{ChR2/WT}$
396 mice for optogenetic stimulations. C57BL/6RJ mice were used for PGE2 and sulprostone
397 exogenous applications, control optogenetic experiments and single-cell RT-PCR. 16-21
398 postnatal day-old females and males were used for all *ex vivo* experiments. Female
399 Emx1$^{cre/WT}$;Ai32$^{ChR2/WT}$ mice, 3 to 5-month-old, were used for *in vivo* experiments.

400 All experimental procedures using animals were carried out in strict accordance with French
401 regulations (Code Rural R214/87 to R214/130) and conformed to the ethical guidelines of
402 the European Communities Council Directive of September 22, 2010 (2010/63/UE). Mice
403 were fed *ad libitum* and housed in a 12-hour light/dark cycle. *In vivo* experiments were done
404 in accordance with the Institut national de la santé et de la recherche médicale (Inserm)
405 animal care and approved by the ethical committee Charles Darwin (Comité national de
406 réflexion éthique sur l'expérimentation animale – n°5) (protocol number #27135
407 2020091012114621).

408 ***Ex vivo* slice preparation**

409 Mice were deeply anesthetized by isoflurane (IsoVet, Piramal Healthcare UK or IsoFlo,
410 Axience) evaporation in an induction box then euthanized by decapitation. The brain was
411 quickly removed and placed in cold (~4°C), oxygenated artificial cerebrospinal fluid (aCSF)
412 containing (in mM): 125 NaCl, 2.5 KCl, 1.25 NaH2PO4, 2 CaCl2, 1 MgCl2, 26 NaHCO3, 10
413 glucose, 15 sucrose and 1 kynurenic acid (Sigma-Aldrich). 300 µm-thick coronal slices
414 containing the barrel cortex were cut with a vibratome (VT1000s; Leica) and were allowed to
415 recover at room temperature for at least 45 min with oxygenated aCSF (95% O2/5% CO2)[39].
416 The slices were then transferred to a submerged recording chamber and continuously
417 perfused at a rate of 2 ml/min with oxygenated aCSF lacking kynurenic acid.

418 **Whole-cell recordings**

419 Patch pipettes (5.5 ± 0.2 MΩ) pulled from borosilicate glass were filled with 8 µl of RNase
420 free internal solution containing (in mM): 144 K-gluconate, 3 MgCl2, 0.5 EGTA, 10 HEPES, pH

421 7.2 (285/295 mOsm). For electrophysiological recordings combined with calcium imaging,
422 EGTA was replaced by 200 µM Rhod-2 (20777, Cayman chemicals). Whole-cell recordings
423 were performed at room temperature (20-25 °C) using a patch-clamp amplifier (Axopatch
424 200B, MDS). Data were filtered at 5-10 kHz and digitized at 50 kHz using an acquisition board
425 (Digidata 1440, MDS) attached to a personal computer running pCLAMP 10.2 software
426 package (MDS). Electrophysiological properties were determined in current-clamp mode[28].
427 Membrane potential values were corrected for theoretical liquid junction potential (−15.6
428 mV). Resting membrane potential of neurons was measured immediately after passing in
429 whole-cell configuration. Only neurons with a resting membrane potential more
430 hyperpolarized than −60 mV were analyzed further.

431 **Optogenetic stimulation**

432 Optogenetic stimulation was achieved through the objective using a 470 nm light emitting
433 device (LED, CoolLED, Precise Excite) attached to the epifluorescence port of a BX51WI
434 microscope (Olympus) and a set of multiband filters consisting of an excitation filter (HC
435 392/474/554/635, Semrock), a dichroic mirror (BS 409/493/573/652, Semrock), and an
436 emission filter (HC 432/515/595/730, Semrock). Photostimulation consisted of a 10-s train of
437 5 ms light pulses at an intensity of 38 mW/mm² and delivered at five different frequencies
438 (1, 2, 5, 10 and 20 Hz).

439 **Infrared imaging**

440 Blood vessels and cells were observed in slices under infrared illumination with Dodt
441 gradient contrast optics (IR-DGC, Luigs and Neumann) using a double-port upright
442 microscope (BX51WI, Olympus) and a collimated light emitting device (LED; 780 nm;
443 ThorLabs) as the transmitted light source, a 40X (LUMPlanF/IR, 40X/0.80 W, Olympus) or a
444 60X (LUMPlan FL/IR 60X/0.90 W, Olympus) objective and a digital camera (OrcaFlash 4.0,
445 Hamamatsu) attached to the front port of the microscope. Penetrating arterioles in layer I
446 were selected by IR-DGC videomicroscopy based on their well-defined luminal diameter (10-
447 40 µm), their length remaining in the focal plane for at least 50 µm[22], and the thickness of
448 their wall (4.1 ± 0.1 µm, n = 176 blood vessels). A resting period of at least 30 min[38] was
449 observed after slice transfer. After light-induced responses, arteriolar contractility was
450 tested by the application of aCSF containing the thromboxane A2 agonist, U46619 (100
451 nM)[16] or K^+ enriched solution (composition in mM: 77.5 NaCl, 50 KCl, 1.25 NaH2PO4, 2 CaCl2,

452 1 MgCl2, 26 NaHCO3, 10 glucose, 15 sucrose). Vessels that did not constrict with these
453 applications were discarded. Only one arteriole was monitored per slice. IR-DGC images
454 were acquired at 0.1 Hz for pharmacological applications and at 1 Hz for optogenetic
455 experiments using Imaging Workbench 6.1 software (Indec Biosystems). The focal plane was
456 continuously maintained on-line using IR-DGC images of cells as anatomical landmarks[22].

457 **Calcium imaging**

458 Visually and electrophysiologically identified layer II-III pyramidal cells were filled with the
459 calcium-sensitive dye Rhod-2 (200 µM, Cayman chemicals, 20777) using patch pipettes.
460 Optical recordings were made at least 15 min after passing in whole-cell configuration to
461 allow for somatic diffusion of the dye. Rhod-2 was excited with a 585 nm LED (Cool LED,
462 Precise Excite) at an intensity of 0.56 mW/mm² and the filter set used for optogenetic
463 stimulation using the Imaging Workbench 6.1 software (Indec Byosystems). IR-DGC and
464 fluorescence images were acquired by alternating epifluorescence and transmitted light
465 sources. IR-DGC and fluorescence were respectively sampled at 5 Hz and 1 Hz during
466 baseline and optogenetic stimulation, respectively, and at 1 Hz and 0.2 Hz after
467 photostimulation. During photostimulation, bleed-through occurred in the Rhod-2 channel
468 due to the fluorescence of the EYFP-ChR2 transgene[26]. Therefore, the Ca^{2+} response could
469 not be reliably analyzed during this period. To compensate for potential x-y drifts, all images
470 were registered off-line using the "StackReg" plug-in[61] of the ImageJ 1.53 software. To define
471 somatic regions of interest (ROIs), the soma was manually delineated from IR-DGC images.
472 Fluorescence intensity changes ($\Delta F/F_0$) were expressed as the ratio $(F-F_0)/F_0$ where F is the
473 mean fluorescence intensity in the ROI at a given time point, and F_0 is the mean fluorescence
474 intensity in the same ROI during the 30-s control baseline.

475 **Drugs**

476 All pharmacological compounds were bath applied after a 5-min baseline, and vascular
477 dynamics were recorded during bath application. The following drugs were dissolved in
478 water: D-(-)-2-amino-5-phosphonopentanoic acid (D-AP5, 50 µM, Hellobio, HB0225), 6,7-
479 dinitroquinoxaline-2,3-dione (DNQX, 10µM, Hellobio, HB0262), LY367385 (100µM, Hellobio,
480 HB0398) and BIBP3226 (1 µM, Tocris, 2707). Tetrodotoxin (TTX, 1 µM, L8503, Latoxan) was
481 dissolved in 90 % acetic acid. PGE2 (HB3460, Hellobio), sulprostone (10 µM, Cayman
482 chemical, 14765), 2-methyl-6-(phenylethynyl)pyridine (MPEP, 50 µM, Hellobio, HB0426) and

483 9,11-dideoxy-9α,11α-methanoepoxy prostaglandin F2α (U-46619, 100 nM, Enzo, BML-
484 PG023) were dissolved in ethanol. Indomethacin (5 µM, Sigma-Aldrich, I7378), SC-560 (100
485 nM, Sigma-Aldrich, S2064-5MG), NS-398 (10 µM, Enzo, BML-EI261), ONO-8130 (10 nM,
486 Tocris, 5406), L-798,106 (1 µM, Cayman chemical, 11129), AL8810 (10 µM, Cayman chemical,
487 16735), paxilline (10 µM, Tocris, 2006) and HET0016 (100 µM, Merck, SML2416-5MG) in
488 DMSO. Acetic acid, ethanol and DMSO doses were always used below 0.1%. Synthesis
489 inhibitors and BIBP3226 were applied at least 30 minutes before optogenetic stimulation.
490 TTX was applied at least 15 minutes before, while glutamate receptor antagonists and
491 paxilline were applied at least 10 and 5 minutes before, respectively.

492 **Vascular reactivity analysis**

493 To compensate for potential x-y drifts, all images were realigned off-line using the
494 "StackReg" plug-in[61] of the ImageJ 1.53 software. Luminal diameter was measured in layer I
495 on registered images using custom analysis software developed in MATLAB (MathWorks)[22].
496 To avoid potential drawbacks due to vessel instability, only arterioles with a stable diameter
497 were analyzed further. Arterioles were considered stable if the relative standard deviation of
498 their diameter during the baseline period was less than 5%[22]. Comparison of the mean
499 arteriolar diameter during the 5-minute baseline and the 5-minute final pharmacological
500 treatments revealed that all drugs, except AL8810, had no effect on resting diameter
501 (Supplementary Fig. 4, 6 and 8).

502 Diameter changes ($\Delta D/D_0$) were expressed as $(D_t - D_0)/D_0$ where D_t is the diameter at the
503 time t and D_0 is the mean diameter during the baseline period. To eliminate sharp artifacts
504 due to transient loss of focus, diameter change traces were smoothed using a sliding three-
505 point median filter. The overall vascular response over time was captured by the area under
506 the curve of diameter changes after photostimulation. Graphs were generated using R
507 software version 4.3.0[62] and Matplotlib package[63].

508 **Intrinsic optical signals analysis**

509 Variations in IR light transmittance (ΔT)[30] were determined using ImageJ 1.53 software
510 according to: $\Delta T = (T_t - T_0)/ T_0$ where T_t is the light transmittance at a time t and T0 is the
511 average light transmittance during the baseline period of a squared region of interest of 100
512 µm x 100 µm manually delineated in layer I. The rate of ΔT change was determined as the
513 first derivative of ΔT ($d\Delta T/dt$, where ΔT is the change in light transmittance and t is time).

514 Slices that showed a maximum rate of increase of dΔT/dt greater than 2%/s, indicating the
515 occurrence of spreading depression[30], were excluded.

516 **Surgery**

517 Chronic cranial windows were implanted one week after the head bar surgery as previously
518 described[64]. We used a 100 µm thick glass coverslip over the barrel cortex (~3mm^2). Before
519 two-photon experiments, a recovery period of 7-10 days minimum was maintained.

520 **Two-photon imaging and photostimulation**

521 For two-photon excitation, we used a femtosecond laser (Mai Tai eHP; SpectraPhysics) with
522 a dispersion compensation module (Deepsee; SpectraPhysics) emitting 70-fs pulses at 80
523 MHz. The laser power was attenuated by an acousto-optical modulator (AA Optoelectronic,
524 MT110-B50-A1.5-IR-Hk). Scanning was performed with Galvanometric scanner (GS) mirrors
525 (8315KM60B; Cambridge Technology). Fluorescein was excited at 920 nm and the emitted
526 light was collected with a LUMFLN60XW (Olympus, 1.1 NA) water immersion objective.
527 Collected photons were sorted using a dichroic mirror centered at 570 nm, a FF01-525/25
528 nm filter (Semrock) and a GaAsP (Hamamatsu) photomultipliers tube. Customized LabView
529 software was used to control the system. Line-scan were drawn across pial vessels to
530 measure diameter change.

531 Mice were anesthetized with a mixture of ketamine and medetomidine (100 and 0.5 mg⁄kg,
532 respectively, intraperitoneal (i.p.)) during imaging sessions. Body temperature was
533 maintained at 36.5°C using a retro-controlled heating pad. Fluorescein dextran (70 kDa) was
534 injected i.v. through a retro-orbital injection to label brain vessels. Mice received continuous
535 air through a nose cone supplemented with oxygen to reach a final concentration of 30% O_2.
536 Photostimulation was delivered with a 473 nm laser (Coblot MLD, Sweden) through an optic
537 fiber placed above the glass coverslip and directed at the pial artery of interest. Each
538 photostimulation consisted of a 10-s train of 5 ms light pulses delivered at 10 Hz, respecting
539 a 5 minutes interstimulus interval. Indomethacin (10mg/kg, #15425529, Thermo Fisher
540 Scientific) was administered i.v. through a retroorbital injection.

541 **Imaging analysis**

542 Pial arteriole diameter change was determined with line-scan acquisitions and a home-made
543 Matlab script as previously described[11]. Trials from the same vessel were averaged (with a

544 0.1 s interpolation) for analysis. Area under the curve and statistics were performed using
545 GraphPad Prim (version 6).

546 **Cytoplasm harvesting and single-cell RT-PCR**

547 At the end of the whole-cell recording, which lasted less than 15 min, the cytoplasmic
548 content was collected in the recording pipette by applying a gentle negative pressure. The
549 pipette's content was expelled into a test tube and RT was performed in a final volume of 10
550 µl as described previously[39]. The scRT-PCR protocol was designed to probed simultaneously
551 the expression of prostaglandins synthesizing enzymes and neuronal markers[22].
552 Prostaglandins synthesizing enzymes included COX-1 and COX-2, the terminal PGE2
553 synthases (PGES): mPGES1, mPGES2 and cPGES, the terminal PGF2α synthases (PGFS): PM-
554 PGFS (Prxl2b) and AKR1B3 and the carbonyl reductase CBR1. Neuronal markers included the
555 vesicular glutamate transporter, vGluT1, and the two isoforms of glutamic acid
556 decarboxylase, GAD65 and GAD67. Two-step amplification was performed essentially as
557 described[39]. First, cDNAs present in the 10 µl reverse transcription reaction were
558 simultaneously amplified with all external primer pairs listed in Supplementary table 2. Taq
559 polymerase (2.5 U; Qiagen) and external primers mix (20 pmol each) were added to the
560 manufacturer's buffer (final volume, 100 µl), and 20 cycles (95◦C, 30 s; 60◦C, 30 s; and 72◦C,
561 35 s) of PCR were performed. Second rounds of PCR were performed using 1 µl of the first
562 PCR product as a template. In this second round, each cDNA was amplified individually using
563 its specific nested primer pair (Supplementary table 2) by performing 35 PCR cycles (as
564 described above). 10 µl of each individual PCR product were run on a 2% agarose gel stained
565 with ethidium bromide using ΦX174 digested by *HaeIII* as a molecular weight marker. The
566 efficiency of the protocol was validated using 500 pg of total forebrain RNAs (Supplementary
567 Fig. 5).

568 **Statistical analyses**

569 Statistical analyses were performed using GraphPad Prism version 7.00 for Windows
570 (GraphPad Software, La Jolla California USA, www.graphpad.com) and R software version
571 4.3.0[62]. Normality of distribution was assessed using the Shapiro-Wilk tests. Equality of
572 variance was assessed using Brown-Forsythe tests for comparisons between groups and
573 using F-tests for comparisons with a control group. Parametric tests were only used if these
574 criteria were met. Statistical significance of morphological and physiological properties of

575 penetrating arterioles was determined using one-way ANOVA for comparison between
576 groups. Statistical significance of calcium was determined using two-tailed unpaired t-tests
577 and Statistical significance of vascular responses were appreciated using Tukey posthoc tests
578 for the different frequencies conditions and using Dunnett's posthoc tests for the different
579 pharmacological conditions compared to the 20 Hz condition without pharmacological
580 compound. False discovery rate correction was used for multiple comparisons. Statistical
581 significance of vascular diameter for drug applications was determined using two-tailed
582 paired t-tests. Statistical significance on all figures uses the following convention: *$p<0.05$,
583 **$p<0.01$ and ***$p<0.001$.

584 **Data availability statement**

585 The data that support the results of this study are available from the corresponding author
586 upon reasonable request.

587 **Acknowledgements**

588 The authors thank Dr Rebecca Piskorowski for constructive criticism of the manuscript. We
589 acknowledge the invaluable support of the animal facilities of IBPS (RongIBPS) and Institut
590 de la vision for their expert care and maintenance of the animals used in this study. Financial
591 support was provided by grants from the Agence Nationale pour la Recherche (ANR-17-
592 CE37-0010-03, B.C.; CE37_2020_TF-fUS-CADASIL, S.C.; ANR-20-CE14-0025, D.L.; ANR-23-
593 CE14-0038-01, B.C.), the Fondation Alzheimer France (M21JRCN009, S.C.) and the i-Bio
594 initiative of Sorbonne University (B.C.). B.L.G. and E.B. were supported by fellowships from
595 Fondation pour la Recherche sur Alzheimer and M.T. by a fellowship from the Fondation
596 pour la Recherche Médicale (SPF201909009103).

597 **Author contributions**

598 B.L.G., M.T., and E.B. designed experiments, acquired, and analyzed the data, and edited the
599 manuscript. S.P. acquired the data. B.L.G. and B.C. drafted the manuscript. I.D. edited the
600 manuscript. H.S. analyzed the data. D.L. designed experiments and edited the manuscript.
601 S.C. and B.C. designed experiments and edited the manuscript.

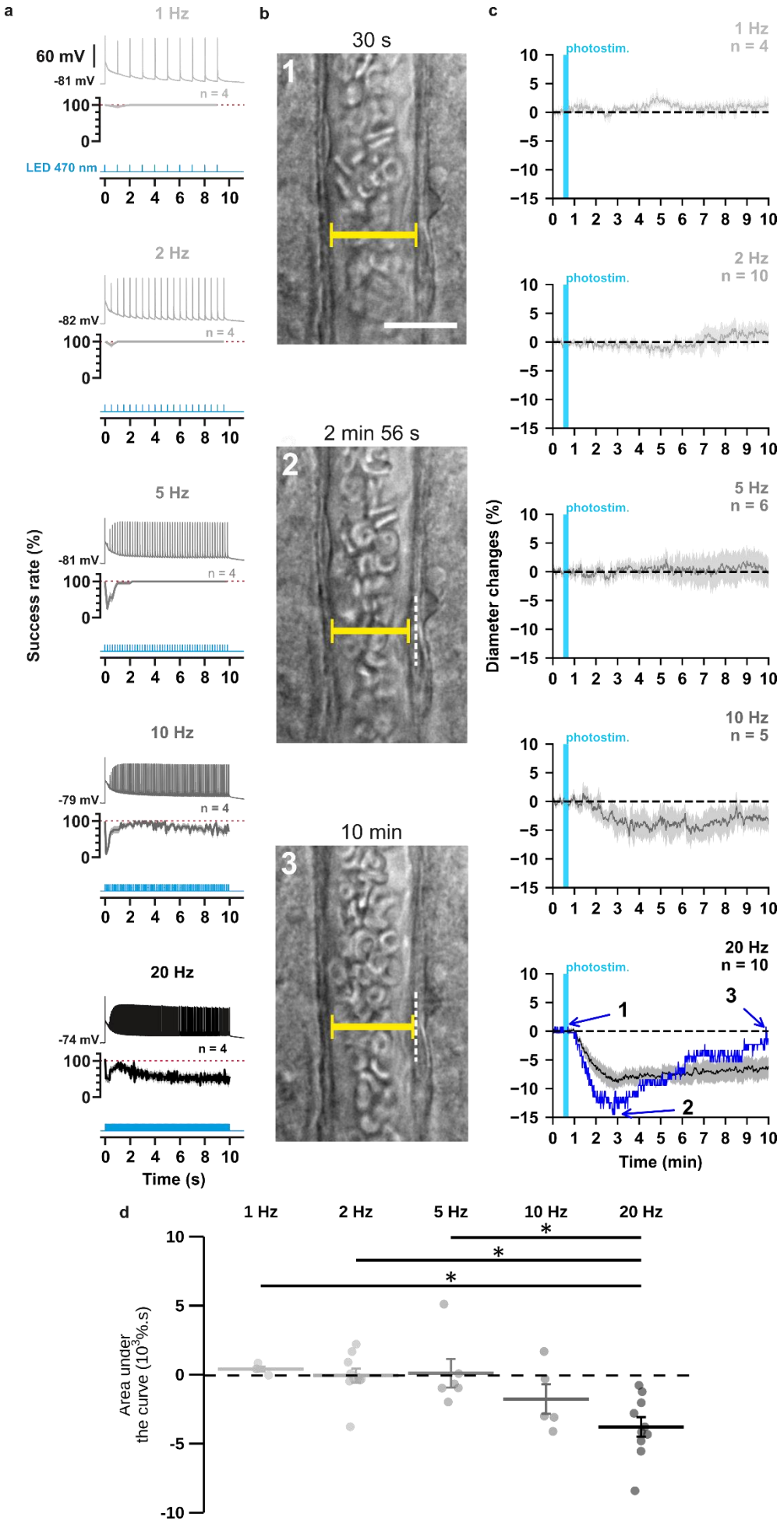
a
1 Hz
60 mV
-81 mV
n = 4
100
0
LED 470 nm
0 2 4 6 8 10
2 Hz
-82 mV
n = 4
5 Hz
-81 mV
n = 4
10 Hz
-79 mV
n = 4
20 Hz
-74 mV
n = 4
Success rate (%)
Time (s)
b
30 s
1
2 min 56 s
2
10 min
3
c
1 Hz
n = 4
photostim.
2 Hz
n = 10
5 Hz
n = 6
10 Hz
n = 5
20 Hz
n = 10
Diameter changes (%)
Time (min)
d
1 Hz
2 Hz
5 Hz
10 Hz
20 Hz
Area under the curve (10³%.s)

Figure 1: The occurrence and strength of vasoconstriction depends on the photostimulation frequency of pyramidal cells. (a) Representative examples of the voltage responses of a layer II-III pyramidal cell (upper traces light grey to black traces) induced by photostimulations (470 nm, 10 s train, 5 ms pulses) delivered at 1, 2, 5, 10 and 20 Hz (cyan lower traces) and mean spike success rate (middle trace, n= 4 cells from 3 mice). The SEMs envelope the mean traces. The red dashed lines represent a spike success rate of 100%. **(b)** Representative example showing IR-DGC pictures of a layer I penetrating arteriole (1) before a 20 Hz photostimulation, (2) at the maximal diameter decrease, and (3) after 10 minutes of recording. Pial surface is upward. Yellow calipers represent the measured diameters. White dashed lines indicate the initial position of the vessel wall. Scale bar: 25 µm. **(c)** Kinetics of arteriolar diameter changes induced by photostimulation (vertical cyan bars) at 1 Hz (n= 4 arterioles from 3 mice), 2 Hz (n= 10 arterioles from 8 mice), 5 Hz (n= 6 arterioles from 6 mice), 10 Hz (n= 5 arterioles from 5 mice) and 20 Hz (n= 10 arteriole from 9 mice). The SEMs envelope the mean traces. The blue trace represents the kinetics of the diameter changes of the arteriole shown in (b). **(d)** Effects of the different photostimulation frequencies on AUC of vascular responses during 10 min of recording. Data are presented as the individual values and mean ± SEM. * statistically different from 20 Hz stimulation with $p<0.05$.

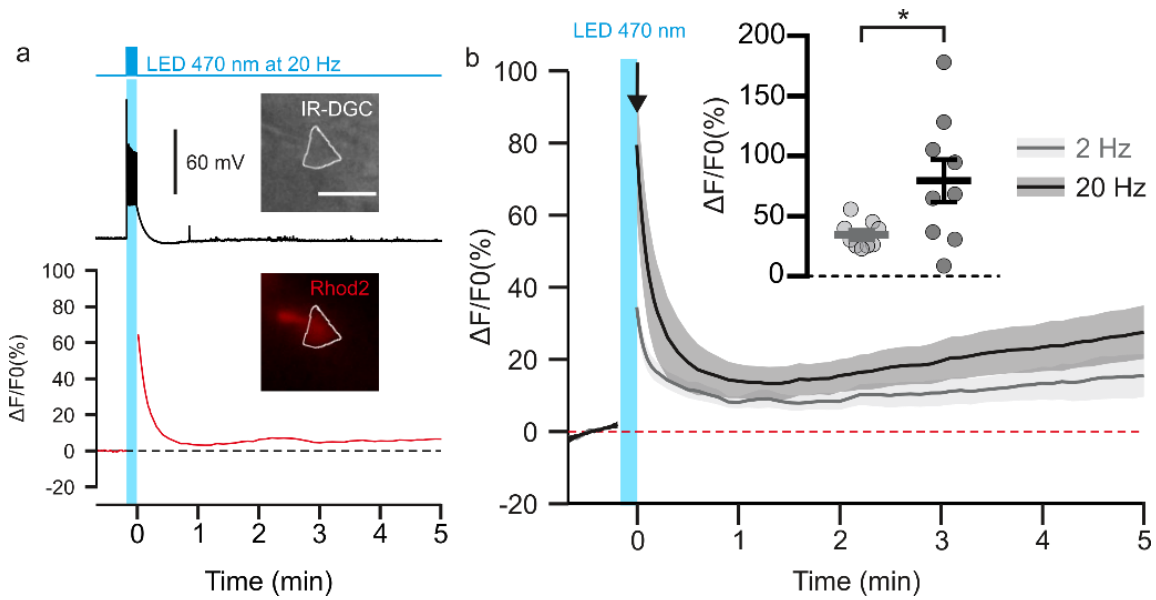

Figure 2: Photostimulation of pyramidal cells elicits a time-locked firing and a frequency-dependent calcium increase. (**a**). Voltage response (top trace) and kinetics of relative fluorescence changes (red bottom trace) induced by photostimulation at 20 Hz. Insets, IR-DGC (top), Rhod2 fluorescence (bottom) pictures of an imaged layer II/III pyramidal cell. The somatic region of interest is outlined in white. Pial surface is upward. Scale bar: 20 µm. **(b)** Mean relative variations of Ca^{2+} fluorescence in response to photostimulation at 2 Hz (grey) and 20 Hz (black). Dashed line represents the baseline. The vertical cyan bar indicates the duration of photostimulation. SEMs envelope the mean traces. Inset, Maximum increase in relative fluorescence changes induced immediately after photostimulation, indicated by the black arrow. The data are shown as the individual values and mean ± SEM. * statistically different with $p < 0.05$.

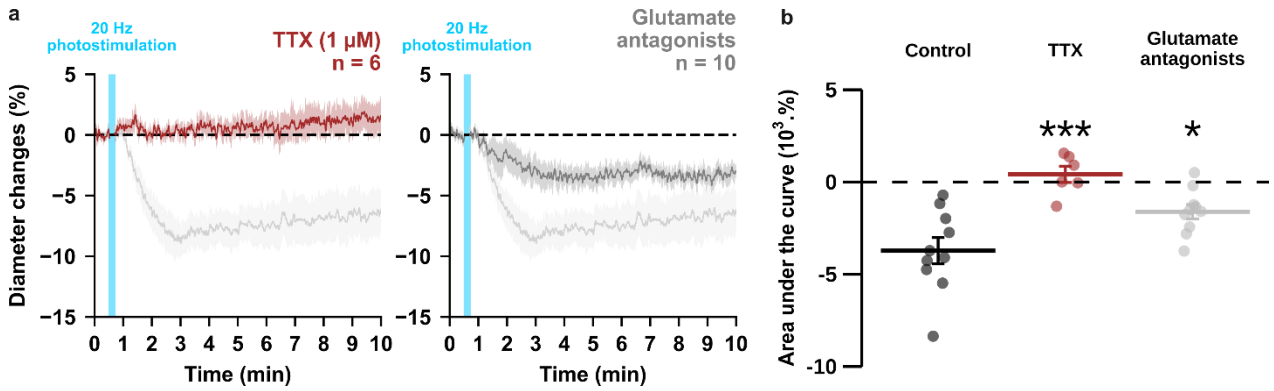

Figure 3: Optogenetically-induced vasoconstriction requires spiking activity and partially glutamatergic transmission. Effect of TTX (1 µM, brown, n= 6 arterioles from 5 mice) and cocktail antagonists of AMPA/kainate (DNQX, 10 µM), NMDA (D-AP5, 50 µM), mGluR1 (LY367385, 100 µM) and mGluR5 (MPEP, 50 µM) receptors (gray, n= 10 arterioles from 6 mice) on **(a)** kinetics and **(b)** magnitude of arteriolar vasoconstriction induced by 20 Hz photostimulation (cyan bar). The SEMs envelope the mean traces. Dashed lines represent the initial diameter. The shadow traces correspond to the kinetics of arteriolar vasoconstriction in control condition. Data are presented as the individual values and mean ± SEM. * and *** statistically different from control condition with $p<0.05$ and $p<0.001$, respectively.

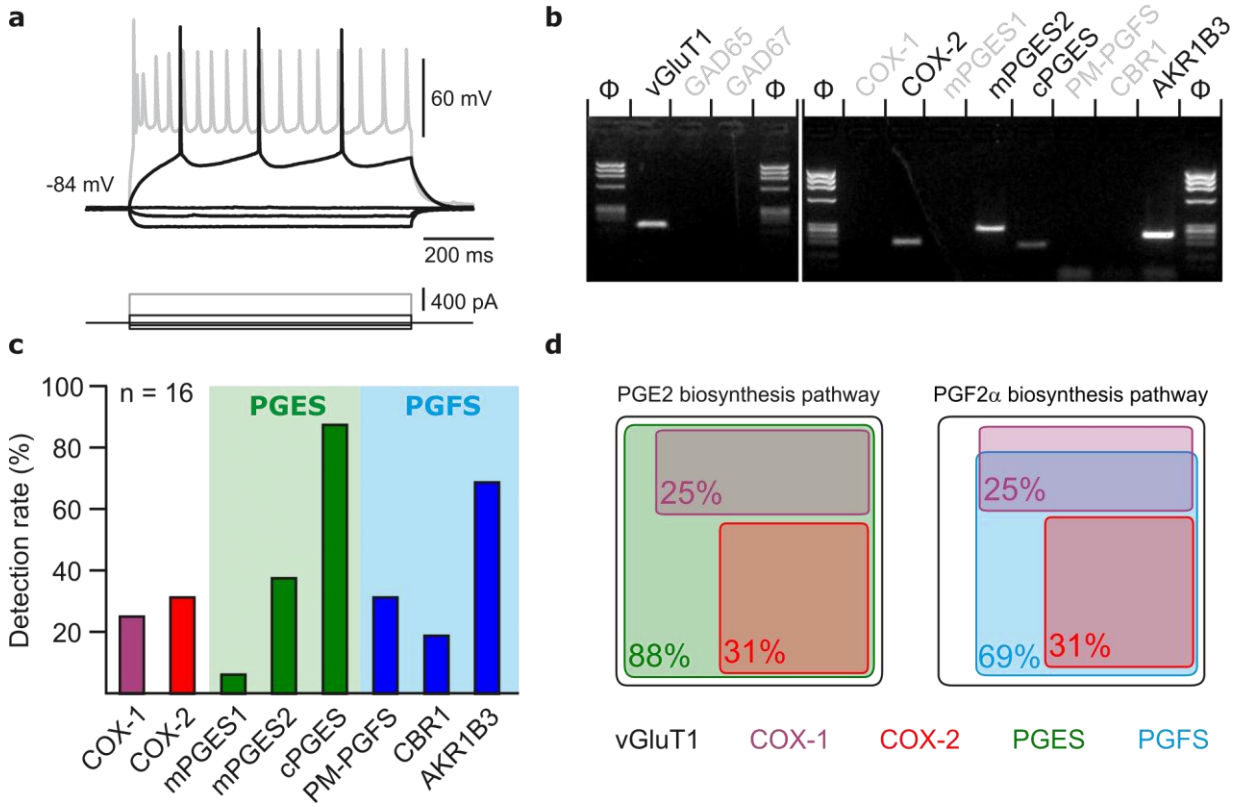

Figure 4: Layer II-III pyramidal cells express PGE2 and PGF2α synthesizing enzymes. (a) Voltage responses of a layer II-III pyramidal cell induced by injection of current (bottom traces). In response to a just-above-threshold current pulse, the neuron fired long-lasting action potentials with little frequency adaptation (middle black trace). Near saturation, it exhibits the pronounced spike amplitude accommodation and marked frequency adaptation characteristic of regular spiking cells (upper grey trace). **(b)** Agarose gel analysis of the scRT-PCR products of the pyramidal cell shown in (**a**) revealing expression of vGluT1, COX-2, mPGES2, cPGES, PM-PGFS and CBR1. Φx174 digested by *HaeIII* (Φ) was used as molecular weight marker **(c)** Histogram summarizing the single-cell detection rate of PGE2 and PGf2α synthesizing enzymes in layer II-III pyramidal cells (n= 16 cells from 6 mice). PGES (green zone) corresponds to mPGES1, mPGES2 and/or cPGES and PGFS (blue zone) to PM-PGFS, CBR1 and/or AKR1B3. **(d)** Co-expression of PGE2 and PGf2α synthesizing enzymes in pyramidal cells. The box size is proportional to the detection rate. Note the absence of co-expression between COX-1 (purple) and COX-2 (red). Co-expression of a PGES (left, green) and a PGFS (right, blue) with COX-1 (up) and COX-2 (bottom).

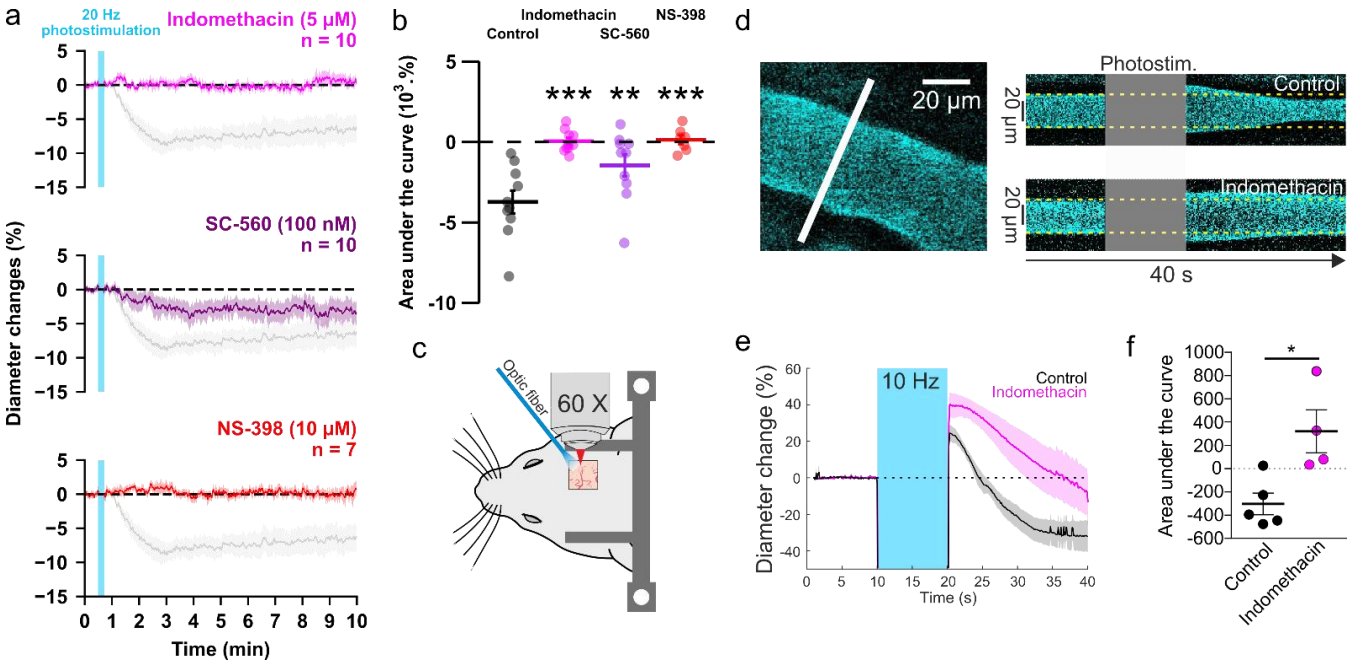

Figure 5: PGE2 mostly derived from COX-2 activity mediates vasoconstriction induced by optogenetically activated pyramidal cells. (a, b) Effects of the COX inhibitors indomethacin (magenta, n= 10 arterioles from 9 mice), SC-560 (purple, n= 10 arterioles from 7 mice) and NS-398 (red, n= 7 arterioles from 6 mice) on kinetics **(a)** and AUC **(b)** of arteriolar vasoconstriction induced by 20 Hz photostimulation (vertical cyan bar). **(c)** Optogenetic stimulation was achieved in vivo with an optic fiber through a chronic cranial window over the barrel cortex. **(d)** Right, diameter change of pial arterioles labeled with fluorescein dextran (i.v) were measured with line-scan crossing the vessel (white line). Left, Representative examples of dilation upon photostimulation (10 Hz, 10 s) under control (top) or indomethacin condition (bottom). **(e)** Diameter changes upon photostimulation under control (black; n = 5 arterioles, 4 mice) or indomethacin (magenta; n = 4 arterioles, 4 mice) conditions. **(f)** Area under the curve of the diameter change in control (black) or indomethacin (magenta) conditions calculated between 20 and 40 s (unpaired, two-tailed Mann Whitney test, * $p<0.05$). The data are shown as the individual values and mean ± SEM. Dashed line represents the baseline. The SEMs envelope the mean traces. The data are shown as the individual values and mean ± SEM. The shadow traces correspond to the control condition. *, ** and *** statistically different from 20 Hz control condition with $p< 0.05$, 0.01 and 0.001, respectively.

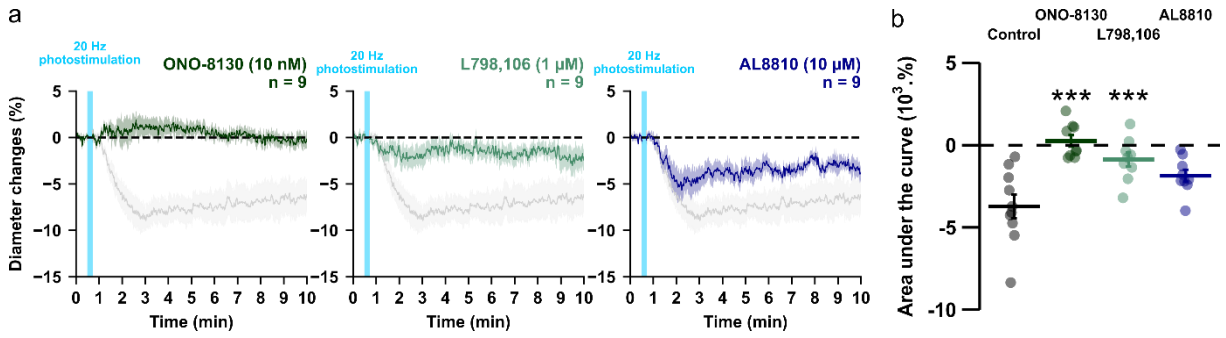

Figure 6: Activation of PGE2 EP1 and EP3 receptors is essential for inducing vasoconstriction triggered by optogenetically activated pyramidal cells. (a, b) Effects of the EP1, EP3 and FP antagonists, ONO-8130 (10 nM, dark green, n= 9 arterioles from 7 mice), L798,106 (1 µM, light green, n= 9 arterioles from 5 mice) and AL8810 (10 µM, dark blue, n= 9 arterioles from 7 mice), respectively, on kinetics **(a)** and AUC **(b)** of arteriolar vasoconstriction induced by 20 Hz photostimulation. Dashed line represents the baseline. The SEMs envelope the mean traces. The data are shown as the individual values and mean ± SEM. The shadow traces correspond to the control condition. *** statistically different from 20 Hz control condition with p< 0.001.

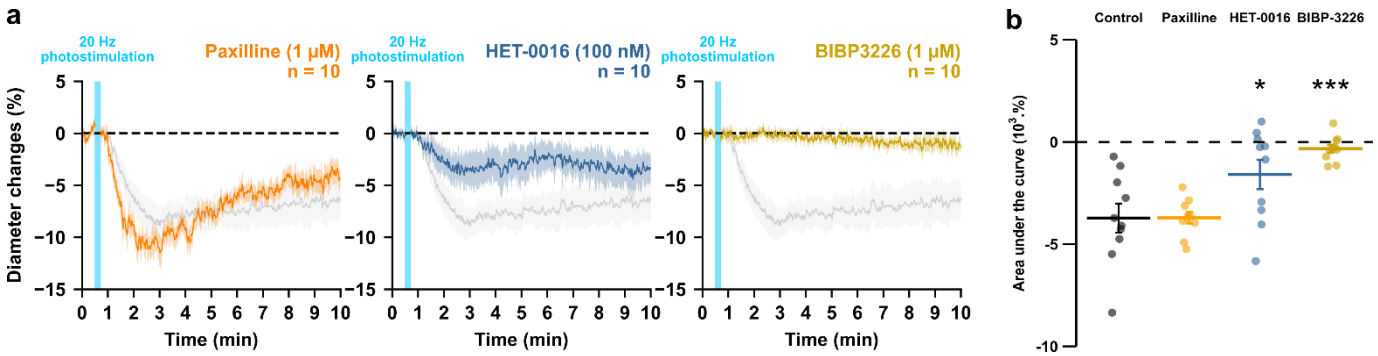

Figure 7: NPY Y1 receptors activation and 20-HETE synthesis mediates the vasoconstriction induced by pyramidal neurons. Effects of paxilline (1 µM, orange, n= 10 arterioles from 6 mice), HET-0016 (100 nM, blue-grey, n= 10 arterioles from 7 mice) and BIBP3226 (1 µM, yellow, n= 10 arterioles from 6 mice) on **(a)** kinetics and **(b)** AUC of arteriolar vasoconstriction induced by 20 Hz photostimulation (vertical blue bar). Dashed line represents the baseline. The SEMs envelope the mean traces. The shadow traces correspond to the control condition. The data are shown as the individual values and mean ± SEM. * and *** statistically different from 20 Hz control condition with $p < 0.05$ and 0.001.

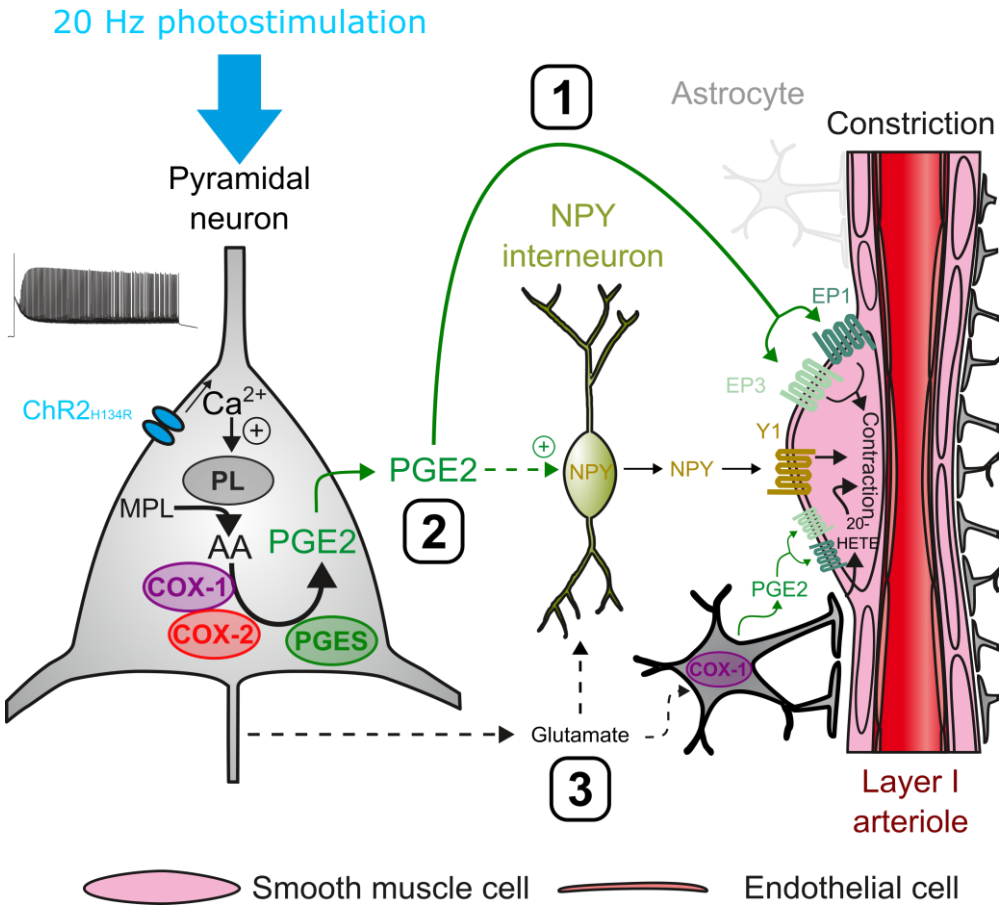

Figure 8: Possible pathways of vasoconstrictions induced by pyramidal neurons. 20 Hz photostimulation induces activation of pyramidal neurons expressing channelrhodopsin-2 ($ChR2_{H134R}$) and elevations of intracellular calcium (Ca^{2+}). Arachidonic acid (AA) is released from membrane phospholipids (MPL) by phospholipases (PL) activated by intracellular Ca^{2+} and metabolized by type-1 and type-2 cyclooxygenases (COX-1 and COX-2) and prostaglandin E2 synthases (PGES) to produce prostaglandin E2 (PGE2). Three possible pathways can be proposed here for the induction arterioles vasoconstriction in layer I: 1) PGE2 released into the extracellular space directly acts on arteriolar EP1 and EP3 receptors to induce constriction of smooth muscle cells. 2) PGE2 activates interneurons and neuropeptide Y (NPY) is released to act on Y1 receptors on smooth muscle cells. 3) Glutamate released by pyramidal cells activates interneurons and astrocytes. Activated astrocytes can induce constriction by the 20-HETE and the COX-1/PGE2 pathways. The three pathways are not exclusive and may act in concert.

References

1. Schmid, F., Barrett, M. J. P., Jenny, P. & Weber, B. Vascular density and distribution in neocortex. Neuroimage 197, 792–805 (2019).

2. Iadecola, C. The Neurovascular Unit Coming of Age: A Journey through Neurovascular Coupling in Health and Disease. *Neuron* **96**, 17–42 (2017).

3. Devor, A. *et al.* Suppressed Neuronal Activity and Concurrent Arteriolar Vasoconstriction May Explain Negative Blood Oxygenation Level-Dependent Signal. *Journal of Neuroscience* **27**, 4452–4459 (2007).

4. Shmuel, A. *et al.* Sustained negative BOLD, blood flow and oxygen consumption response and its coupling to the positive response in the human brain. *Neuron* **36**, 1195–1210 (2002).

5. O'Herron, P. *et al.* Neural correlates of single-vessel haemodynamic responses in vivo. *Nature* **534**, 378–382 (2016).

6. Ma, Y. *et al.* Resting-state hemodynamics are spatiotemporally coupled to synchronized and symmetric neural activity in excitatory neurons. *Proceedings of the National Academy of Sciences* (2016) doi:10.1073/pnas.1525369113.

7. Devor, A. *et al.* Stimulus-Induced Changes in Blood Flow and 2-Deoxyglucose Uptake Dissociate in Ipsilateral Somatosensory Cortex. *Journal of Neuroscience* **28**, 14347–14357 (2008).

8. Uhlirova, H. *et al.* Cell type specificity of neurovascular coupling in cerebral cortex. *Elife* **5**, 1–23 (2016).

9. Farrell, J. S. *et al.* Postictal behavioural impairments are due to a severe prolonged hypoperfusion/ hypoxia event that is COX-2 dependent. (2016) doi:10.7554/eLife.19352.001.

10. Tran, C. H. T., George, A. G., Teskey, G. C. & Gordon, G. R. Seizures elevate gliovascular unit Ca2+ and cause sustained vasoconstriction. *JCI Insight* **5**, (2020).

11. Rungta, R. L., Chaigneau, E., Osmanski, B. F. & Charpak, S. Vascular Compartmentalization of Functional Hyperemia from the Synapse to the Pia. *Neuron* 1–14 (2018) doi:10.1016/j.neuron.2018.06.012.

12. Hill, R. A. *et al.* Regional Blood Flow in the Normal and Ischemic Brain Is Controlled by Arteriolar Smooth Muscle Cell Contractility and Not by Capillary Pericytes. *Neuron* **87**, 95–110 (2015).

13. Hartmann, D. A. *et al.* Brain capillary pericytes exert a substantial but slow influence on blood flow. *Nat Neurosci* **24**, 633–645 (2021).

14. Rungta, R. L. *et al.* vascular arbors in layer II / III somatosensory cortex. *Commun Biol* (2021) doi:10.1038/s42003-021-02382-w.

15. Zhang, D. *et al.* Synaptic-like transmission between neural axons and arteriolar smooth muscle cells drives cerebral neurovascular coupling. *Nat Neurosci* 1–17 (2024) doi:10.1038/s41593-023-01515-0.

16. Cauli, B. *et al.* Cortical GABA interneurons in neurovascular coupling: Relays for subcortical vasoactive pathways. *Journal of Neuroscience* **24**, 8940–8949 (2004).

17. Mulligan, S. J. & MacVicar, B. A. Calcium transients in astrocyte endfeet cause cerebrovascular constrictions. *Nature* **431**, 195–199 (2004).

18. Girouard, H. *et al.* Astrocytic endfoot Ca2+ and BK channels determine both arteriolar dilation and constriction. *Proc Natl Acad Sci U S A* **107**, 3811–3816 (2010).

19. Lecrux, C. *et al.* Pyramidal Neurons Are 'Neurogenic Hubs' in the Neurovascular Coupling Response to Whisker Stimulation. *Journal of Neuroscience* **31**, 9836–9847 (2011).

20. Gordon, G. R. J., Choi, H. B., Rungta, R. L., Ellis-Davies, G. C. R. & MacVicar, B. A. Brain metabolism dictates the polarity of astrocyte control over arterioles. *Nature* **456**, 745–9 (2008).

21. Mishra, A. *et al.* Astrocytes mediate neurovascular signaling to capillary pericytes but not to arterioles. *Nat Neurosci* **19**, 1619–1627 (2016).

22. Lacroix, A. *et al.* COX-2-Derived Prostaglandin E2 Produced by Pyramidal Neurons Contributes to Neurovascular Coupling in the Rodent Cerebral Cortex. *J Neurosci* **35**, 11791–11810 (2015).

23. Rosehart, A. C. *et al.* Prostaglandin E2 Dilates Intracerebral Arterioles When Applied to Capillaries: Implications for Small Vessel Diseases. *Front Aging Neurosci* **13**, 1–11 (2021).

24. Dabertrand, F. *et al.* Prostaglandin E2, a postulated astrocyte-derived neurovascular coupling agent, constricts rather than dilates parenchymal arterioles. *Journal of Cerebral Blood Flow and Metabolism* **33**, 479–482 (2013).

25. Gorski, J. A. *et al.* Cortical excitatory neurons and glia, but not GABAergic neurons, are produced in the Emx1-expressing lineage. *Journal of Neuroscience* **22**, 6309–6314 (2002).

26. Madisen, L. *et al.* A toolbox of Cre-dependent optogenetic transgenic mice for light-induced activation and silencing. *Nat Neurosci* **15**, 793–802 (2012).

27. Lin, J. Y., Lin, M. Z., Steinbach, P. & Tsien, R. Y. Characterization of engineered channelrhodopsin variants with improved properties and kinetics. *Biophys J* **96**, 1803–1814 (2009).

28. Karagiannis, A. *et al.* Classification of NPY-expressing neocortical interneurons. *J Neurosci* **29**, 3642–59 (2009).

29. Chung, D. Y. *et al.* Determinants of Optogenetic Cortical Spreading Depolarizations. *Cerebral Cortex* **29**, 1–12 (2018).

30. Zhou, N., Gordon, G. R. J., Feighan, D. & MacVicar, B. A. Transient swelling, acidification, and mitochondrial depolarization occurs in neurons but not astrocytes during spreading depression. *Cerebral Cortex* **20**, 2614–2624 (2010).

31. Rungta, R. L., Osmanski, B.-F., Boido, D., Tanter, M. & Charpak, S. Light controls cerebral blood flow in naive animals. *Nat Commun* **8**, 14191 (2017).

32. Attwell, D. *et al.* Glial and neuronal control of brain blood flow. *Nature* **468**, 232–43 (2010).

33. Cauli, B. & Hamel, E. Revisiting the role of neurons in neurovascular coupling. *Front Neuroenergetics* **2**, 9 (2010).

34. Smetters, D., Majewska, A. & Yuste, R. Detecting action potentials in neuronal populations with calcium imaging. *Methods: A Companion to Methods in Enzymology* **18**, 215–221 (1999).

35. Tasic, B. *et al.* Adult mouse cortical cell taxonomy revealed by single cell transcriptomics. *Nat Neurosci* **advance on**, 1–37 (2016).

36. Zeisel, A. *et al.* Cell types in the mouse cortex and hippocampus revealed by single-cell RNA-seq. *Science (1979)* **347**, 1138–1142 (2015).

37. Sun, W. *et al.* Glutamate-Dependent Neuroglial Calcium Signaling Differs Between Young and Adult Brain. *Science (1979)* **339**, 197–200 (2013).

38. Zonta, M. *et al.* Neuron-to-astrocyte signaling is central to the dynamic control of brain microcirculation. *Nat Neurosci* **6**, 43–50 (2003).

39. Devienne, G., Le Gac, B., Piquet, J. & Cauli, B. Single Cell Multiplex Reverse Transcription Polymerase Chain Reaction After Patch-Clamp. *Journal of Visualized Experiments* **136**, 1–12 (2018).

40. Sharif, N. A. & Klimko, P. G. Prostaglandin FP receptor antagonists: discovery, pharmacological characterization and therapeutic utility. *Br J Pharmacol* **176**, 1059–1078 (2019).

41. Boie, Y. *et al.* Molecular cloning and characterization of the four rat prostaglandin E 2 prostanoid receptor subtypes. 227–241 (1997).

42. Clasadonte, J. *et al.* Prostaglandin E 2 release from astrocytes triggers gonadotropin-releasing hormone (GnRH) neuron firing via EP2 receptor activation. *Proc Natl Acad Sci U S A* **108**, 16104–16109 (2011).

43. Di Cesare, A., Del Piccolo, P., Zacchetti, D. & Grohovaz, F. EP2 receptor stimulation promotes calcium responses in astrocytes via activation of the adenylyl cyclase pathway. *Cellular and Molecular Life Sciences* **63**, 2546–2553 (2006).

44. Kahn, I. *et al.* Optogenetic drive of neocortical pyramidal neurons generates fMRI signals that are correlated with spiking activity. *Brain Res* **1511**, 33–45 (2013).

45. Scott, N. A. & Murphy, T. H. Hemodynamic responses evoked by neuronal stimulation via channelrhodopsin-2 can be independent of intracortical glutamatergic synaptic transmission. *PLoS One* **7**, 1–10 (2012).

46. Blanco, M., Stern, J. E. & Filosa, J. A. Tone-dependent vascular responses to astrocyte-derived signals. *American journal of physiology.* 2855–2863 (2008) doi:10.1152/ajpheart.91451.2007.

47. Mao, B. Q., Hamzei-Sichani, F., Aronov, D., Froemke, R. C. & Yuste, R. Dynamics of spontaneous activity in neocortical slices. *Neuron* **32**, 883–898 (2001).

48. Niwa, K., Araki, E., Morham, S. G., Ross, M. E. & Iadecola, C. Cyclooxygenase-2 contributes to functional hyperemia in whisker-barrel cortex. *Journal of Neuroscience* **20**, 763–770 (2000).

49. Desai, S., April, H., Nwaneshiudu, C. & Ashby, B. Comparison of agonist-induced internalization of the human EP2 and EP4 prostaglandin receptors: role of the carboxyl terminus in EP4 receptor sequestration. *Mol Pharmacol* **58**, 1279–86 (2000).

50. Kasischke, K. A. *et al.* Two-photon NADH imaging exposes boundaries of oxygen diffusion in cortical vascular supply regions. *Journal of Cerebral Blood Flow and Metabolism* **31**, 68–81 (2011).

51. Yamagata, K., Andreasson, K. I., Kaufmann, W. E., Barnes, C. A. & Worley, P. F. Expression of a Mitogen-Inducible Cyclooxygenase in Brain Neurons : Regulation by Synaptic Activity and Glucocorticoids. *Neuron* **11**, 371–386 (1993).

52. Yamagata, K. *et al.* Coexpression of microsomal-type prostaglandin E synthase with cyclooxygenase-2 in brain endothelial cells of rats during endotoxin-induced fever. *Journal of Neuroscience* **21**, 2669–2677 (2001).

53. Takemiya, T., Matsumura, K. & Yamagata, K. Roles of prostaglandin synthesis in excitotoxic brain diseases. *Neurochem Int* **51**, 112–120 (2007).

54. Takei, S. *et al.* Immunohistochemical demonstration of increased prostaglandin F2α levels in the rat hippocampus following kainic acid-induced seizures. *Neuroscience* **218**, 295–304 (2012).

55. Bao, L. *et al.* Localization of neuropeptide Y Y1 receptors in cerebral blood vessels. *Proc Natl Acad Sci U S A* **94**, 12661–6 (1997).

56. Attwell, D., Mishra, A., Hall, C. N., O'Farrell, F. M. & Dalkara, T. What is a pericyte? *Journal of Cerebral Blood Flow and Metabolism* **36**, 451–455 (2016).

57. Krawchuk, M. B., Ruff, C. F., Yang, X., Ross, S. E. & Vazquez, A. L. Optogenetic assessment of VIP, PV, SOM and NOS inhibitory neuron activity and cerebral blood flow regulation in

mouse somato-sensory cortex. *Journal of Cerebral Blood Flow and Metabolism* **40**, 1427–1440 (2020).

58. Lee, J. *et al.* Opposed hemodynamic responses following increased excitation and parvalbumin-based inhibition. *Journal of Cerebral Blood Flow and Metabolism* (2020) doi:10.1177/0271678X20930831.

59. Zhang, D. Y. & Raichle, M. E. Disease and the brain's dark energy. *Nat Rev Neurol* **6**, 15–28 (2010).

60. Palop, J. J. & Mucke, L. Amyloid-B-induced neuronal dysfunction in Alzheimer's disease: From synapses toward neural networks. *Nat Neurosci* **13**, 812–818 (2010).

61. Thévenaz, P., Ruttimann, U. E. & Unser, M. A pyramid approach to subpixel registration based on intensity. *IEEE Transactions on Image Processing* **7**, 27–41 (1998).

62. R Core Team. R: A Language and Environment for Statistical Computing. Preprint at (2023).

63. Caswell, T. A. *et al.* matplotlib/matplotlib: REL: v3.7.2. (2023) doi:10.5281/ZENODO.8118151.

64. Tournissac, M. *et al.* Cranial window for longitudinal and multimodal imaging of the whole mouse cortex. *Neurophotonics* **9**, 1–13 (2022).